The Hybrid Bidirectional DC/DC Converter

Mutual Control and Stability Analysis

Liu, Haiyang; Cui, Shumei; Zhang, Hanwen; Hu, Yiwen; Xue, Yuhongyang; Liu, Chuang

Published in:
CSEE Journal of Power and Energy Systems

DOI (link to publication from Publisher):
10.17775/CSEEJPES.2021.00260

Publication date:
2023

Document Version
Publisher's PDF, also known as Version of record

The Hybrid Bidirectional DC/DC Converter: Mutual Control and Stability Analysis

Haiyang Liu, Shumei Cui, *CSEE*, *Member*, Hanwen Zhang, Yiwen Hu, Yuhongyang Xue, and Chuang Liu, *CSEE*, *Member*

***Abstract*—A hybrid bidirectional DC/DC converter (BDC) is proposed as the fundamental DC/DC module in solid-state transformers, which combines a bidirectional LLC converter and a dual-active-bridge (DAB) converter. Integrated with a mutual control scheme, both parts of this hybrid BDC can be unified into an interdependent community. In this hybrid BDC, the LLC converter supports the output voltage and improves stability by working at the resonant frequency mode and the DAB converter enhances the BDC power capability by controlling the LLC output current constant. The BDC can achieve the full-load-range soft switching of all active switches by designing the auxiliary inductor of LLC and the minimum output current of DAB. By comparing to the single DAB, the proposed BDC has the higher phase and gain margin which means the BDC improved the relative stability based on Nyquist criterion. To solve the bidirectional power control problem, a dead-band voltage control logic is adopted which can determine the BDC's power direction based on the output voltage change. A 200 V experimental system has verified the aforementioned features and functions of the BDC.**

***Index Terms*—Bidirectional DC-DC converter, mutual control.**

I. Introduction

POWER electronics transformers (PETs), which are called solid-state transformers (SSTs) as well, have become the critical devices in the smart grid of the future for achieving power distribution among different voltage AC&DC buses [1]–[6] and also have some potential additional functions, such as harmonic filter, reactive power compensation, etc. To achieve the electrical isolation, the high voltage ratio, the low volume and the weight, PETs usually contain multiple bidirectional DC/DC converters (BDCs) with a high-frequency (HF) transformer.

In most PET topologies [1]–[5], [7], [8], the BDC normally utilizes the phase-shift modulated dual-active-bridge (DAB) converter on account of its simple structure, high bidirectional power capacity and Zero Voltage Switching (ZVS) for all switches. However, the simple and feasible single-phase-shift (SPS) DAB limits the ZVS range and low-load efficiency, especially when high voltage is required [9]. For the SPS DAB, the ZVS range is generally contradictory with its switching current stress [10]. Although wide bandgap devices can alleviate this problem, an increase in industrial costs is inevitable. Several improved DAB control methods improve efficiency, expand the ZVS's operation range and relieve current stress by using extra control degrees, such as the Extended-Phase-Shift (EPS) [11], [12], the Dual-Phase-Shift (DPS) [13] and the Triple-Phase-Shift (TPS) [14]. However, these control methods are difficult to implement, because it is hard to coordinate these independent control degrees under a unified standard at present [15], [16]. Although some optimized principles have been proposed in [17]–[19], these methods are all based on extremely complex online and offline calculations while the overall detailed parameters are indispensable. Moreover, with a light load condition, the DAB power transmission performs the obvious error with the typical DAB power model because of the dead-time effects [20], and this phenomenon becomes harder to ignore in high frequency applications [21], [22]. Thus, the light load conditions brings obvious challenges to the DAB controller design. The parameter mismatches in transformers always cause unbalance issues for the PET applications, so an extra voltage balancing control has to be used in these cases [23]–[26]. This also produces more pressure for the PET controller.

To avoid the aforementioned DAB problems, some PET topologies use the LLC series resonant converter as the basic module of the DC/DC stage [27], [28]. The LLC converter provides a load-independent operating point with a constant voltage gain at the switching frequency near the resonant frequency [29], and the resonant tank does not allow the LLC t0 be affected very much by the parameter tolerances [30], so the PET achieves the natural voltage sharing by adopting LLC modules [31]–[33]. At any load condition, the LLC converter achieves the primary side ZVS and the secondary side Zero Current Switching (ZCS). However, its forward voltage gain is different than the backward voltage gain. A modified bidirectional LLC converter contains an extra inductor [34], [35] and a CLLC converter, in which one more series resonant capacitor is installed [36]. This topology improves the bidirectional gain characteristics by making the resonant tank symmetrical. Whereas the series resonant capacitor has limited current capacity, neither of the topologies is suitable for high power conditions.

A novel hybrid LLC resonant and DAB linear DC/DC

Manuscript received January 9, 2021; revised March 16, 2021, accepted June 10, 2021. Date of online publication December 30, 2021; date of current version August 24, 2022.

H. Y. Liu (corresponding author, email: lhy1122@126.com) and S. M. Cui are with the School of Electrical Engineering and Automation, Harbin Institute of Technology, Harbin 150001, China.

C. Liu, Y. W. Hu and Y. H. Y. Xue are with the School of Electrical Engineering, Northeast Electric Power University, Jilin 132012, China.

DOI: 10.17775/CSEEJPES.2021.00260

converter is proposed in [37]. It combines the advantages of the LLC converter and the DAB converter with a simple output current control method, which enhances the control stability and achieves the soft switching of all devices throughout the whole load range. At the same time, the hybrid converter voltage gain is dominated by the LLC converter.. However, this hybrid converter is unidirectional and has too many components.

In this paper, a new BDC is proposed based on the topology in [37]. The new BDC not only inherits all the advantages of the hybrid DAB-LLC converter but also achieves bidirectional power flow. For the PET applications, the proposed BDC has 3 main advantages over the DAB converter.

1) The proposed BDC avoids the DAB light-load zone and thus reduces the difficulty of the controller design and improves the module efficiency for the light-load conditions.
2) The proposed BDC has a constant voltage gain which is dominated by the SC converter, so the voltage balancing control is no longer necessary.
3) The proposed BDC, with a mutual control, has higher relative stability than the SPS DAB.

The remainder of this paper is organized as follows. We present more design principles of different parameters in Section II and Section III. In Section IV, the details of the mutual control are analyzed, based on the BDC small-signal model, and the bidirectional control logic, including the principle of changing the power flow direction, is also explained. Section V presents the experimental results to verify the functions of the proposed BDC. The conclusion is presented in Section VI.

II. Topology and Operating Principle of Hybrid Bidirectional DC/DC Converter

Figure 1 shows the circuit diagram of the proposed novel BDC composed of two parts: 1) the DAB converter, including eight MOSFETs (Q_{t1}∼Q_{t8}) forming two full bridges, a high-frequency transformer TR1 with the leakage inductor L_t and the magnetic inductor L_{m1} and the equivalent circuit resister R_t of TR1 and the MOSFETS (Q_{t1}∼Q_{t8}); 2) the bidirectional half-bridge LLC converter, including four MOSFETs (Q_{r1}∼Q_{r4}) forming two half bridges, the high-frequency transformer TR2 with leakage inductor L_r and magnetic inductor L_{m2}, an auxiliary inductor $L_{\rm ma}$, a resonant capacitor C_r and the equivalent circuit resister R_r of TR2, C_r and MOSFETs (Q_{r1}∼Q_{r4}).

To ensure that the LLC output voltage gains are the same in the contrary directions, the auxiliary inductor $L_{\rm ma}$, which is equal to L_{m2}, is added onto the resonant tank side to make the resonant network symmetrical. Fig. 2 shows the equivalent circuit of the bidirectional LLC converter where n_2 is the ratio of TR2.When the switching frequency of the LLC part f_r is equal to the resonant frequency of L_r and C_r, with the fundamental harmonic approximation (FHA) method, the forward gain and backward gain can be expressed [18] as:

$$M_{\text{forward}} = M_{\text{backward}} = \frac{V_o}{V_i} = \frac{1}{n_2} \tag{1}$$

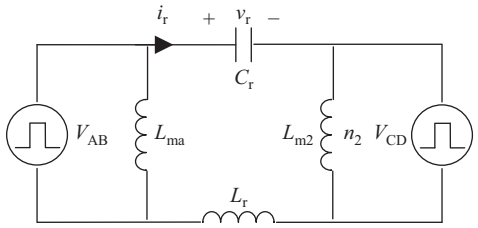

Fig. 2. The equivalent AC circuit of the LLC converter.

Actually, two parts of the proposed BDC are in parallel as shown in Fig. 3. Considering the application of the proposed BDC, a DC voltage source V_i is adopted to simulate the input side which is connected to the DC sides of AC-DC converters or a mass of energy-storage devices. The output side is equivalent to a current source I_s where many renewable generation devices are installed, because photovoltaics and wind energy systems generally work with a maximum power point tracking (MPPT) control strategy.

The BDC has two power directions which are forward direction and backward direction. In either direction of the BDC, there are two modes: 1) single-LLC mode: the LLC operates in open-loop state and 2) LLC-DAB mode: the LLC and the DAB act in parallel, and the LLC output current is

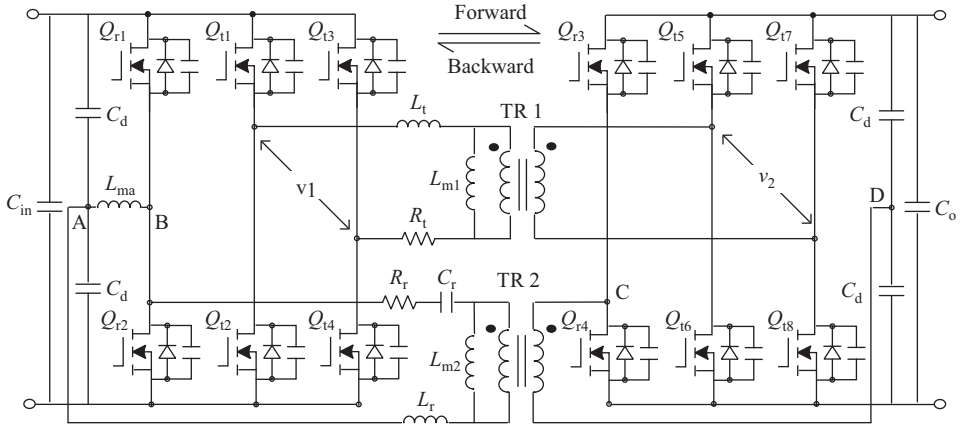

Fig. 1. Circuit schematic of the hybrid bidirectional DC/DC converter.

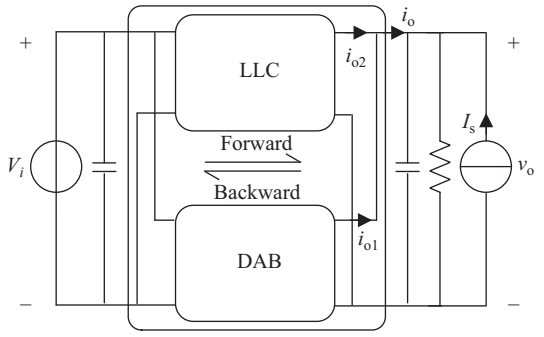

Fig. 3. Sketch of the hybrid bidirectional DC/DC converter.

controlled to the reference I_{ref} by adjusting the DAB phase-shift ratio.

According to the power level, the BDC operating principle is shown in Fig. 4. The limit I_{tmin} is the minimum current which ensures all the DAB switches achieve ZVS. Then, when the BDC output current i_o is lower than the threshold $I_{\text{th}} = I_{\text{tmin}} + I_{\text{ref}}$, the DAB phase-shift ratio must be lower than a certain value $D_{\min}$, the BDC closes all DAB switches and works in the single-LLC mode in this case. The LLC rated output current can be designed as I_{th}, and its rated output power is $P_{\text{ra\_LLC}} = I_{\text{th}} V_o$. When the BDC output current i_o is higher than the threshold $I_{\text{th}} = I_{\text{tmin}} + I_{\text{ref}}$, the BDC works in the LLC-DAB mode. Thus, the DAB output current range is always from I_{tmin} to I_{tra} where I_{tra} is the rated output current of the DAB. Therefore, the DAB guarantees all the switches for ZVS in such a case. The whole BDC rated output current is $I_{\text{ra}} = I_{\text{tra}} + I_{\text{ref}}$. The detailed mode description is shown in the following section.

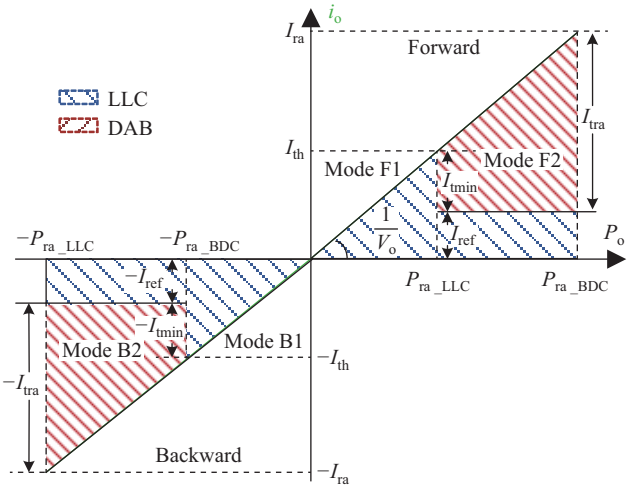

Fig. 4. The diagram of the operating principle.

A. Forward Operating Principle

Mode F1: When the forward power is lower than $P_{\text{ra\_LLC}}$, LLC part works separately, while the DAB converter is off. Thus, the MOSFETs Q_{r1} and Q_{r2} alternatively switch at the resonant frequency f_r and other MOSFETs are all off. The output DC voltage v_o depends on the LLC forward gain M_{forward}. At this time, all power only flows through the LLC converter and the output current i_o is equal to the LLC output current i_{o2}.

Mode F2: The DAB onverter begins to work with the LLC converter together, when the forward power increases and i_o exceeds the threshold I_{th}. The MOSFETs (Q_{r1}∼Q_{r4}) of the LLC converter still works as mode F1, while the output bridge (Q_{t5}∼Q_{t8}) produces a square voltage which lags a phase-shift ratio d behind the square voltage produced by the input bridge (Q_{t1}∼Q_{t4}). The DAB output current i_{o1} is given in (2).

$$i_{o1} = \frac{p_{\text{DAB}}}{v_o} = \frac{V_i n_1}{2 L_t f_t} d(1-d) \tag{2}$$

where n_1 is the ratio of TR1 and f_t is the DAB frequency. The output current i_o is the sum of i_{o1} and i_{o2}. By adjusting the phase-shift ratio d, the DAB output current i_{o1} will compensate the load changing to make the LLC output current i_{o2} invariant as I_{ref}. In this mode, the output DC voltage for the whole converter is controlled by the constant voltage gain of the LLC converter at all times.

B. Back Operating Principle

When the current source I_s exceeds the requirement for the load on the output side, the BDC will turn into the backward power direction. At this time, the operating principle is similar to that in the forward state as shown in Fig. 4. There are also two modes in the backward state.

Mode B1: If the backward power is insufficient, the LLC converter still works separately. But the MOSFETs Q_{r1} and Q_{r2} are off and the MOSFETs Q_{r3} and Q_{r4} alternatively switch at the resonant frequency f_r. The LLC converter works in the backward state and the voltage v_o obeys the LLC backward gain M_{backward}.

Mode B2: If the negative output current i_o becomes lower than $-I_{\text{th}}$, the DAB converter will start to work, but the phase-shift ratio d will be negative to cause the power flow to be backward. The LLC current i_{o2} is controlled to be equal to $-I_{\text{ref}}$ by adjusting the DAB current i_{o1} and it should be lower than the $-I_{\text{tmin}}$ all the time.

It is obvious that no matter which mode the BDC operates in, v_o is certainly desired by the LLC open-loop gains M_{forward} and M_{backward}.

III. ZVS Condition Analysis and Parameters' Designation

In this hybrid BDC, it is obvious that the auxiliary inductor L_{ma} and the threshold value I_{tmin} directly influence the operating performance. Therefore, based on the accurate ZVS analysis in each part of the BDC, both of the parameters are designed to achieve BDC's ZVS in the whole load range as follows.

A. L_{ma} Configuration

The auxiliary inductor L_{ma} will improve the ZVS performance of LLC, but increase the loop current. Thus, the appropriate inductance value should be designed for the auxiliary inductor. Generally, the LLC converter achieves ZVS using the peak of the transformer magnetizing current I_m [38]. In

the LLC converter of the proposed hybrid BDC, I_m can be derived as:

$$I_m = I_{m1} + I_{m2} \tag{3}$$

where I_{m1} is the peak of TR2 magnetizing current and I_{m2} is the peak of $L_{\rm ma}$ inductor current.

$$I_{m1} = \frac{V_o}{8n_2 f_r L_{m2}} \tag{4a}$$

$$I_{m2} = \frac{V_i}{8f_r L_{\rm ma}} \tag{4b}$$

Figure 5 shows the equivalent circuit of the half-bridge LLC converter during dead time. The C_{r1} and C_{r2} are parasitic switch capacitors, whose capacitance is $C_{\rm oss}$. For a given $T_{\rm dead}$, the required I_m for successful ZVS of the half-bridge is derived as:

$$I_m \geq \frac{2C_{\rm oss}V_i}{T_{\rm dead}} \tag{5}$$

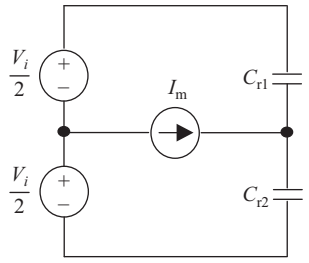

Fig. 5. The equivalent circuit of the half-bridge LLC part during dead-time.

Therefore, with (3)–(5), the inductance of $L_{\rm ma}$ and L_{m2} is obtained as:

$$L_{\rm ma} = L_{m2} \leq \frac{T_{\rm dead}}{8f_r C_{\rm oss}} \tag{6}$$

B. I_{tmin} Setting

The minimum output current directly influences the ZVS performance of the DAB converter. Fig. 6 shows the input bridge equivalent circuit and main waveforms of the DAB converter during dead-time interval $T_{\rm dead}$, which is also the cycle time. When switches Q_{t1} and Q_{t4} turn off at $t = 0$,

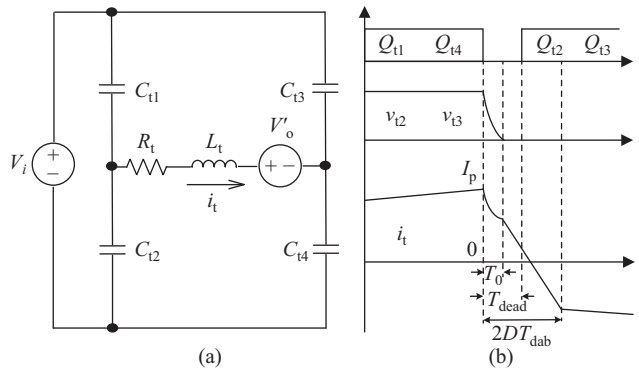

Fig. 6. The (a) input bridge equivalent circuit and (b) main waveforms of DAB converter during dead time.

the input bridge of the DAB converter requires the inductance current i_t to charge the parasitic switch capacitors C_{t1} and C_{t4} while discharging C_{t2} and C_{t3}. Until the voltage of C_{t2} and C_{t3} drops to zero at $t = T_0$, if i_t is still positive, the anti-paralleled diodes turn on clamping the voltage across C_{t2} and C_{t3}. During the interval $0 < t < T_0$

$$V_i - V_o' = v_1 + R_t i_t + L_t \frac{{\rm d}i_t}{{\rm d}\tau} + v_4 \tag{7}$$

From the Kirchhoff laws:

$$C\frac{{\rm d}v_{1,4}}{{\rm d}\tau} = -C\frac{{\rm d}v_{2,3}}{{\rm d}\tau} = \frac{i_t}{2} \tag{8}$$

where C is the value of C_{t1}–C_{t4} and $v_{1,4}$ is the voltage across C_{t1} and C_{t4} and $v_{2,3}$ is the voltage across C_{t2} and C_{t3}. Thus, by substituting (8) into (7), the following equation is derived as:

$$CL_t\frac{{\rm d}^2 v_{2,3}}{{\rm d}\tau^2} + CR_t\frac{{\rm d}v_{2,3}}{{\rm d}\tau} + v_{2,3} = \frac{V_i + V_o'}{2} \tag{9}$$

and at $t = 0$

$$v_{2,3}(0) = V_i, \frac{{\rm d}v_{2,3}}{{\rm d}\tau}(0) = -\frac{I_p}{2C} \tag{10}$$

Combining (9) with (10), the voltage across C_{t2} and C_{t3} is expressed as:

$$v_{2,3} = \frac{V_i - V_o'}{2}\cos(\omega\tau) - \frac{I_p}{2C\omega}\sin(\omega\tau) + \frac{V_i + V_o'}{2} \tag{11}$$

where

$$\omega = \frac{\sqrt{4L_tC - R_t^2C^2}}{2L_tC} \tag{12}$$

To ensure the ZVS, there must be $T_0 \leq T_{\rm dead}$. Thus, from (11) and (12), the minimum peak $I_{\rm pmin}$ is derived as:

$$I_{\rm pmin} = \frac{\omega C((V_i - V_o')\cos(\omega T_{\rm dead}) + V_i + V_o')}{\sin(\omega T_{\rm dead})} \tag{13}$$

According to [28], the peak current of L_t is expressed as:

$$I_p = \frac{V_i - V_o' + 2V_o'\alpha^{(1-D)} - (V_i + V_o')\alpha}{R_t(1+\alpha)} \tag{14}$$

where

$$\alpha = e^{-\frac{R_t}{L_t}T} \tag{15}$$

It is noted that T is the half of the switching period. Referring to (13)–(15), the minimum DAB phase shift ratio for ZVS can be derived as:

$$D_{\rm min} = 1 + \frac{L_t}{TR_t} \ln\left(\frac{R_tI_{\rm pmin}(1+\alpha) + (V_i + V_o')\alpha - V_i + V_o'}{2V_o'}\right) \tag{16}$$

Therefore, referring to (2) and (16), the limitation $I_{\rm tmin}$ which regulates starting of DAB can be derived as:

$$I_{\rm tmin} = \frac{n_1V_i}{2f_tL_t}D_{\rm min}(1 - D_{\rm min}) \tag{17}$$

C. I_{ref} Setting

The current reference I_{ref} is important to make sure the BDC efficiency is not lower than the same-power DAB converter. For the output-voltage-controlled converter, the efficiency function η has the positive correlation with the output current. Therefore, based on the BDC operating principle, the I_{ref} design should meet the following condition as:

$$(1-\eta_{\text{DAB1}})\,\Delta I + (1-\eta_{\text{LLC1}})\,I_{\text{ref}} \le (1-\eta_{\text{DAB2}})\,I_o \tag{18}$$

where

$$\Delta I = I_o - I_{\text{ref}} \tag{19}$$

The η_{DAB1} is the DAB efficiency when its output current is ΔI, η_{DAB2} is the DAB efficiency when its output current is I_o and η_{LLC1} is the LLC efficiency when its output current is I_{ref}. From (18) and (19), the I_{ref} constraint can be derived as:

$$I_{\text{ref}} \ge \frac{\eta_{\text{DAB2}} - \eta_{\text{DAB1}}}{\eta_{\text{LLC1}} - \eta_{\text{DAB1}}} I_o \tag{20}$$

From no load to the rated power, both the LLC and DAB converters usually have the positive correlation between the efficiency and the output power because the fixed transformer core loss rapidly decreases its proportion in the total loss as the power level rises. And the efficiency values have little difference in the high-power level with the same reason. So, to guarantee (20), the LLC design and I_{ref} should match to achieve a high η_{LLC1}.

IV. Mutual Control and Bidirectional Logic

The control target of the proposed BDC is to sustain the output voltage in every mode and to change the power flow direction when required. Thus, the mutual control method is analyzed based on the average model of the BDC and the bidirectional dead-band logic is explained in this section.

A. Modeling

To simplify the mathematical model of this hybrid BDC, some assumptions must be presented. First, the transformers and all switches are ideal. Second, the dynamics of the series voltage divider capacitors C_d are not to be considered that their voltage division is always equal. Third, the transformer magnetizing current is not significant, because the magnetic inductance of each transformer is far larger than the corresponding leakage inductance L_r or L_t.

By referring to Fig. 1, the state equations of the proposed BDC can be derived as:

$$\frac{\mathrm{d}v_o}{\mathrm{d}t} = \frac{|i_r|}{2C_o} - \frac{v_o}{RC_o} + \frac{s_2 i_t}{C_o} \tag{21a}$$

$$\frac{\mathrm{d}i_r}{\mathrm{d}t} = -\frac{v_r}{L_r} - \frac{i_r R_r}{L_r} - \frac{\operatorname{sgn} v_o}{2L_r} + \frac{s_r V_i}{2L_r} \tag{21b}$$

$$\frac{\mathrm{d}v_r}{\mathrm{d}t} = \frac{i_r}{C_r} \tag{21c}$$

$$\frac{\mathrm{d}i_t}{\mathrm{d}t} = \frac{s_1}{L_t} V_i - \frac{s_2 v_o}{L_t} - \frac{i_t R_t}{L_t} \tag{21d}$$

where s_r and sgn are the LLC switching function while s_1 and s_2 are the DAB switching functions. R is the load resistance. With the similar modeling approach proposed in [39]–[41], the small-signal model of the BDC is given in the matrix form

$$\frac{\mathrm{d}x}{\mathrm{d}t} = \boldsymbol{A}x + \boldsymbol{B}\Delta d \tag{22a}$$

$$y = Cx \tag{22b}$$

where

$$\boldsymbol{x} = \left(\Delta v_o, \Delta i_{r1R}, \Delta i_{r1I}, \Delta v_{r1R}, \Delta v_{r1I}, \Delta i_{t1R}, \Delta i_{t1I}\right)^{\mathrm{T}} \tag{23a}$$

$$\boldsymbol{A} = \begin{pmatrix} \frac{-1}{RC_o} & \frac{-k_R}{\pi C_o} & \frac{-k_I}{\pi C_o} & 0 & 0 & \frac{-4\alpha}{\pi C_o} & \frac{-4\beta}{\pi C_o} \\ \frac{-k_R}{\pi L_r} & -m_R & \omega_r & \frac{-1}{L_r} & 0 & 0 & 0 \\ \frac{k_I}{\pi L_r} & -\omega_r & -m_I & 0 & \frac{-1}{L_r} & 0 & 0 \\ 0 & \frac{1}{C_r} & 0 & 0 & \omega_r & 0 & 0 \\ 0 & 0 & \frac{1}{C_r} & -\omega_r & 0 & 0 & 0 \\ \frac{2\alpha}{\pi L_t} & 0 & 0 & 0 & 0 & -\frac{R_t}{L_t} & \omega_t \\ \frac{2\beta}{\pi L_r} & 0 & 0 & 0 & 0 & -\omega_t & -\frac{R_t}{L_t} \end{pmatrix} \tag{23b}$$

$$\boldsymbol{B} = \begin{pmatrix} \frac{4}{C_o}\left(\langle I_{t1}\rangle_R \beta - \langle I_{t1}\rangle_I \alpha\right) \\ 0 \\ 0 \\ 0 \\ 0 \\ \frac{2\langle V_o\rangle_0}{L_t}\beta \\ -\frac{2\langle V_o\rangle_0}{L_t}\alpha \end{pmatrix} \tag{23c}$$

$$\alpha = \sin(D\pi) \tag{23d}$$

$$\beta = \cos(D\pi) \tag{23e}$$

$$k_R = \langle I_r\rangle_{1R} \Big/ \sqrt{\langle I_r\rangle_{1R}^2 + \langle I_r\rangle_{1I}^2} \tag{23f}$$

$$k_I = \langle I_r\rangle_{1I} \Big/ \sqrt{\langle I_r\rangle_{1R}^2 + \langle I_r\rangle_{1I}^2} \tag{23g}$$

$$m_R = R_r + \sqrt{2}k_R V_o \Big/ \left(\pi L_r \sqrt{\langle I_r\rangle_{1R}}\right) \tag{23h}$$

$$m_1 = R_r + \sqrt{2}k_I V_o \Big/ \left(\pi L_r \sqrt{\langle I_r\rangle_{1I}}\right) \tag{23i}$$

The subscripts $\boldsymbol{R}$ and $\boldsymbol{I}$ represent the real and the imaginary parts of a complex number. Then the control-to-current transfer function (TF) of the BDC is given by:

$$G_{id}(s) = C_{id}(sE - A)^{-1}B \tag{24}$$

where s is the Laplace symbol and E is a 7*7 identity matrix, the matrix C_{id} is also demonstrated in [42], [43] as:

$$C_{id} = \left(0, \frac{2}{\pi}k_R, \frac{2}{\pi}k_I, 0, 0, 0, 0\right) \tag{25}$$

Figure 7 shows the Bode diagram of the BDC TF from (24), (25) based on the parameters in Table I and the TF simulation results which match the theoretical calculation. Therefore, the BDC small-signal model is verified.

B. Mutual Control

According to the principle in Section II, the mutual control guarantees the output voltage by LLC open-loop gain and relieves LLC stress with the DAB current control. This mutual control consists of a PI controller, a BDC model G_{id} and the

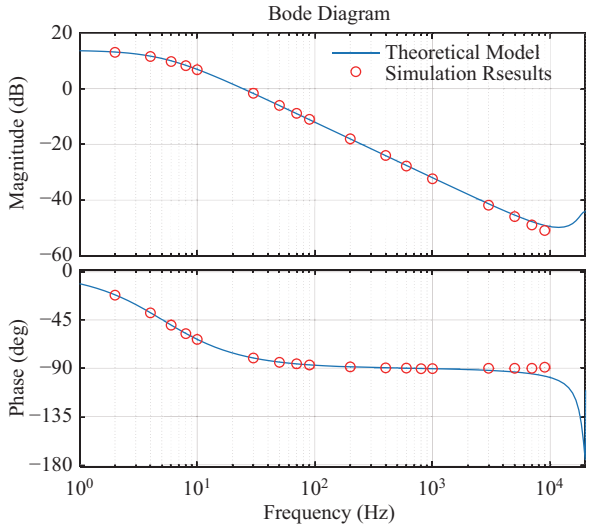

Fig. 7. Bode diagrams of the control-to-current TF.

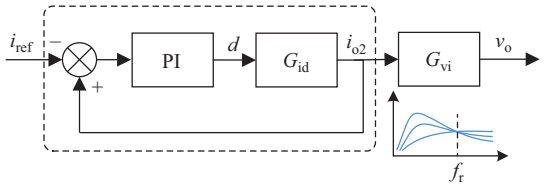

Fig. 8. Mutual control schematic of BDC.

TABLE I
PARAMETERS OF THE BDC

Parameters	Value
L_r	7.2 μH
C_r	1 μF
C_{oss}	220 pF
C	970 pF
L_{ma}	158.3 μH
L_t	37.2 μH
C_d	540 μF
C_o	2.2 mF
R_r	0.1 Ω
R_t	0.3 Ω
f_r	60 kHz
f_t	20 kHz
PI controller	(0.1 s+100)/s

LLC open-loop voltage gain G_{vi} as shown in Fig. 8. The control system in the dashed box produces the requiring i_{o2} which is equal to the reference i_{ref} by adjusting the DAB phase-shift ratio d. Based on the transfer function (24) and the small signal model in [30], Fig. 9 shows the Nyquist diagram of the hybrid BDC and the SPS DAB. The parameters of the SPS DAB are exactly the same to the DAB converter of the BDC in Table I. From Fig. 8, neither curve encircles the point $(-1, j0)$, so according to the Nyquist criterion, both systems are stable. The gain margin K_g and the phase margin γ of both systems are also shown in Fig. 9. It is obvious that $K_{g1} < K_{g2}$ and $\gamma_1 < \gamma_2$, so this intuitively shows that the proposed BDC has a higher relative stability than the SPS DAB converter.

C. Bidirectional Dead-band Logic

Figure 10 shows the entire algorithm of the proposed BDC,

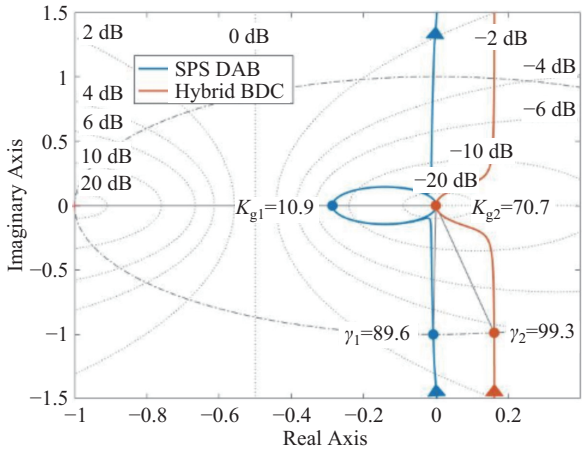

Fig. 9. Nyquist diagrams of hybrid BDC and SPS DAB.

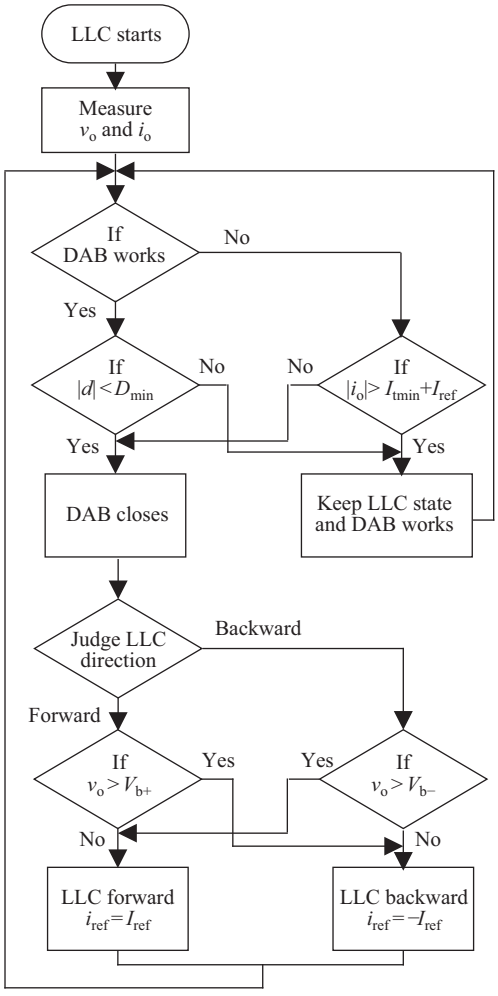

Fig. 10. Total control logic of the proposed BDC.

including the bidirectional dead-band logic [44]. The first step is to decide the DAB state based on the principle shown in Section II. When the DAB is working, the LLC converter maintains the previous state and the procedure goes to the next cycle. If the DAB is off, the LLC will be allowed to change its direction. Fig. 11 shows the theoretical waveform when the LLC changes its direction. When the BDC is in the

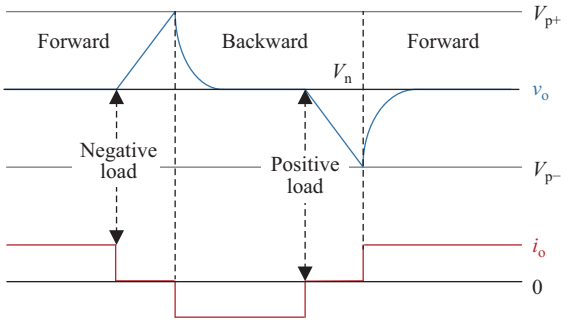

Fig. 11. Theoretical waveform of changing direction.

forward state, i_o declines to zero and v_o inevitably rises for C_o is charging if the load current becomes negative. The LLC state does not change until v_o reaches the upper limit of the permissible voltage range V_{p+}. Then the LLC turns into the backward state and i_{ref} becomes $-I_{\text{ref}}$ to assort with the DAB backward state. The output voltage v_o is restored to the normal value V_{n} and i_o becomes negative. In the same manner, the BDC can be changed from backward state to forward state when v_o reaches V_{p-}.

V. Experimental Result

The main parameters of the proposed BDC are shown in Table I. To verify the performance of the proposed BDC, an experimental system is established. It consists of a 200 V DC voltage source on the input side and a current source on the output side as shown in Fig. 3. The ratio of TR1 and TR2 is 1:1 in this experimental system. The closed-loop reference current I_{ref} is given as 1 A. The dead time T_{dead} is fixed as 400*ns*. Therefore, according to the Eqs. (16) (17), the parameters $D_{\min}$ and I_{tmin} can be calculated as $D_{\min} = 0.021$ and $I_{\text{tmin}} = 2.78$ A. To guarantee the DAB ZVS, the current I_{th} is given as 4 A which is higher than the sum of I_{ref} and I_{tmin}.

Figure 12(a) consists of the waveforms illustrating the BDC transforming from mode F1 to mode F2. The step-up load makes the LLC output current i_{o2} higher than I_{th}, the DAB converter starts to control i_{o2} back to the I_{ref}. The system reaches a new steady state with the DAB phase shift ratio $d = 0.032$. Fig. 12(b) illustrates the waveforms when the load increases from 1 kW to 2 kW in mode F2. It is obvious that the DAB converter increases its output power to match the heavier load and i_{o2} is controlled as I_{ref}. In these two processes, the output voltage v_o remains stable at 200 V. Therefore, Fig. 12 verifies that the BDC steadily follows the forward principles of the BDC as shown in Fig. 4.

Figure 13(a) illustrates the BDC principle of mode conversion from B1 to B2. After the LLC converter turns into the backward state, the reference current I_{ref} becomes -1 A and I_{tmin} becomes -3 A. Thus, when i_{o2} is less than -4 A, the DAB will start with the negative phase-shift ratio to control

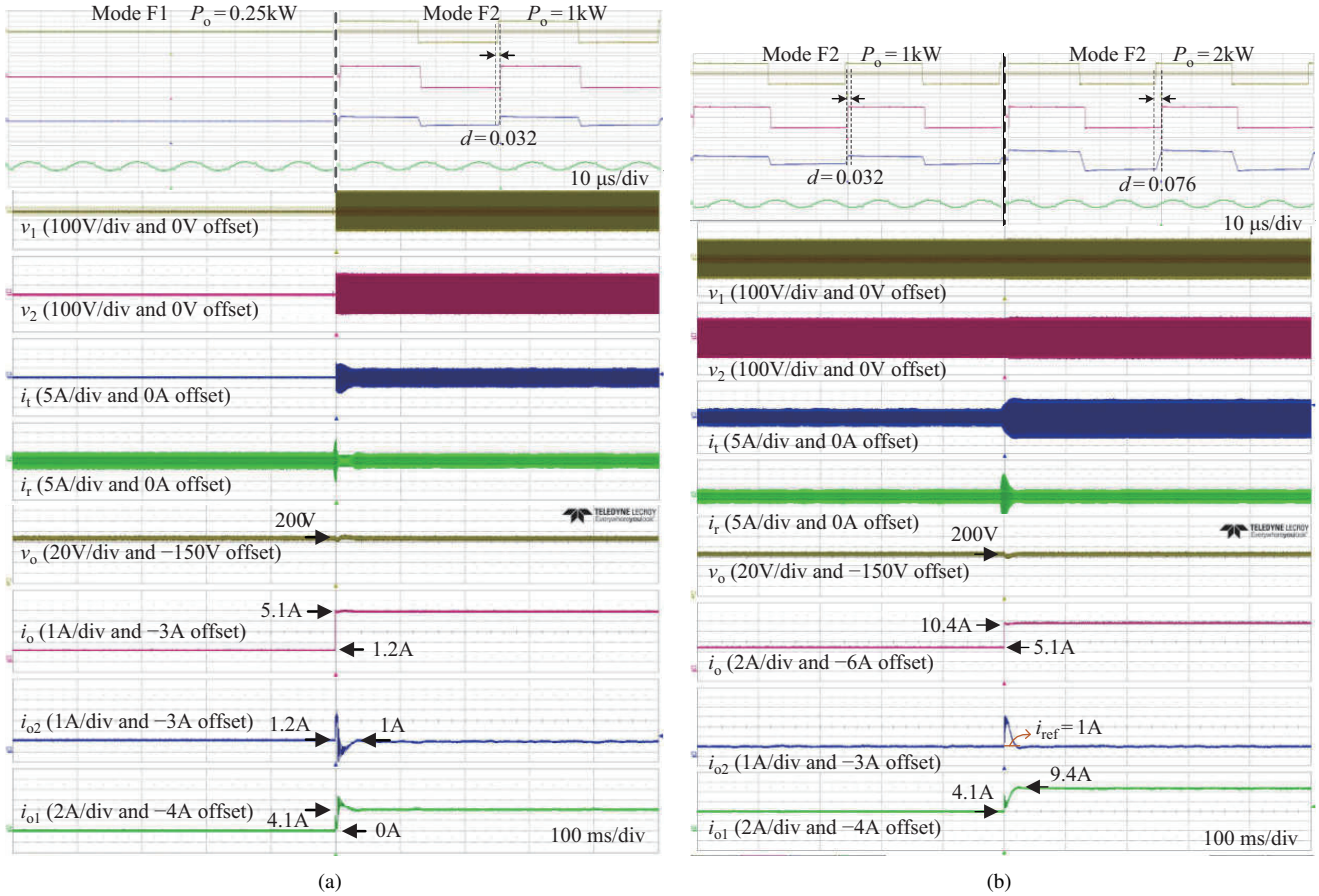

Fig. 12. Load step waveforms in forward direction. (a) Mode F1 to mode F2, (b) 1 kW to 2 kW in mode F2.

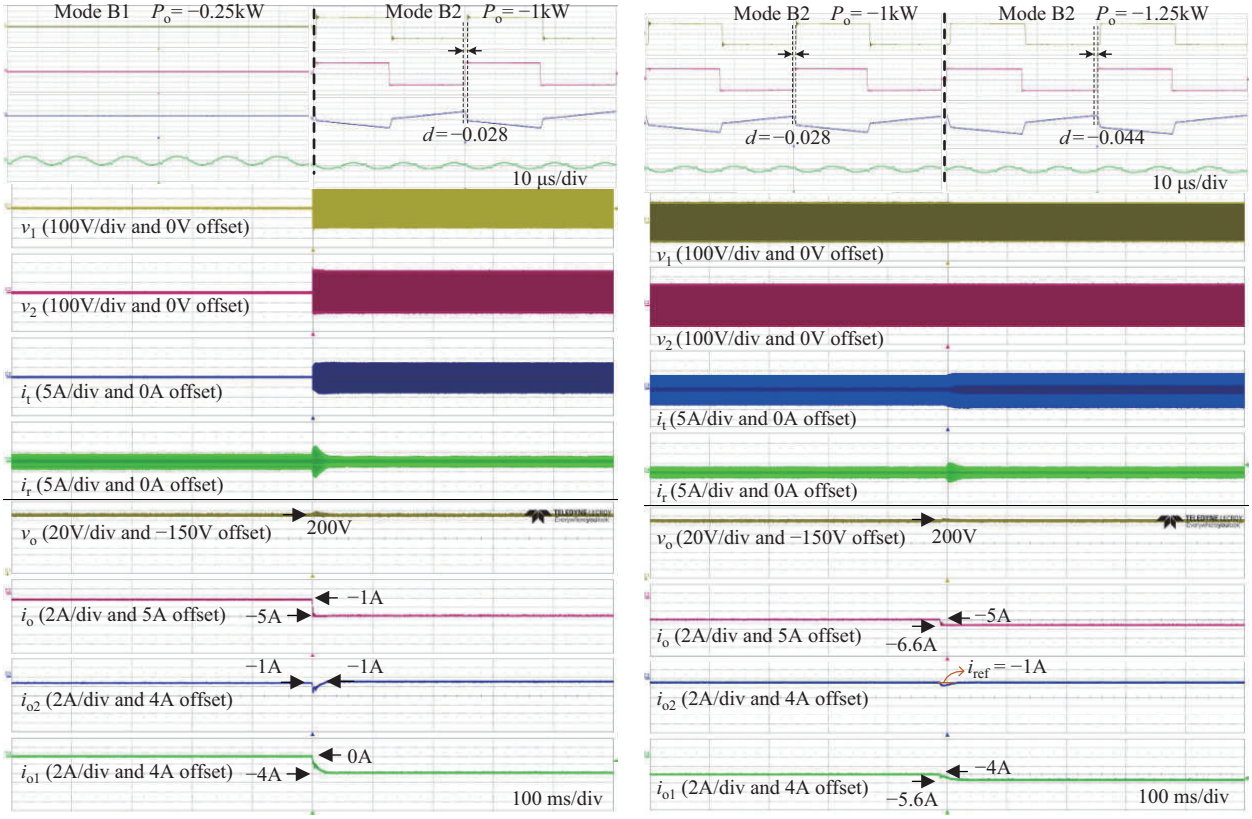

Fig. 13. Load step waveforms in backward direction. (a) Mode B1 to mode B2, (b) −1 kW to −1.25 kW in mode B2.

i_{o2} to be −1 A. Fig. 13(b) verifies the operating principle in mode B2. When the current source increases, the DAB converter adjusts its backward power to coordinate this change. The voltage v_o still stably remains at 200 V in backward state.

Figure 14 shows the waveforms of the BDC power-direction reversion. The permissible voltage range is given as ± 30 V. The whole process is the same as the theoretical waveform in Fig. 11. When the load lightens, the current source causes the output voltage rise until v_o reaches 230 V. During this period, the BDC works in the forward no-load state. Then the BDC turns to mode B1. The i_o becomes negative and v_o is restored to 200 V.

Figure 15 is the measured efficiency curves of the hybrid BDC and an SPS DAB converter, including the forward modes and the backward modes. The parameters of the SPS DAB converter are the same as the DAB converter in the hybrid BDC for effective contrasting. It is evident that the full-load-range soft switching makes the hybrid BDC more efficient than the DAB converter at light load conditions (±0.25 kW to ±0.75 kW). When the BDC turns to mode F2 and B2 at ±1 kW load, the BDC efficiency is slightly lower than the SPS DAB, because the DAB converter power is lower than the SPS DAB at the moment. But with the load power increasing, both curves tend to quickly be the same.

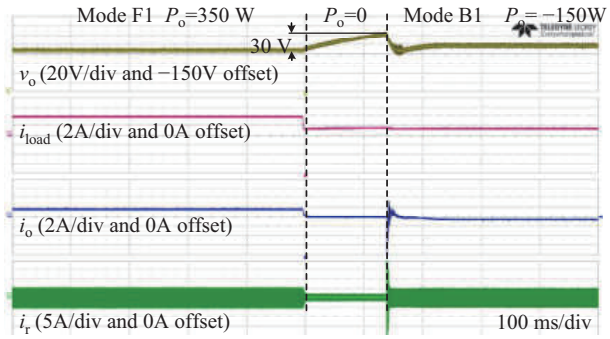

Fig. 14. Waveforms from mode F1 to B1.

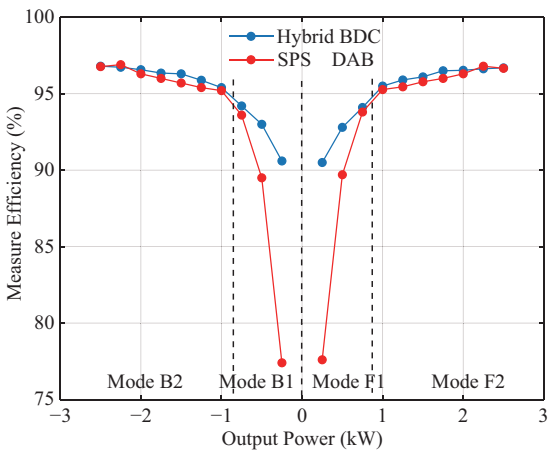

Fig. 15. Measured efficiency of the hybrid BDC and the SPS DAB at V_{in} = 200 V, V_{out} = 200 V.

VI. Conclusion

This paper presents a hybrid bidirectional DC/DC converter for PET, which has a stable output voltage gain and high-power capability. The operating principle and critical parameters design are given to express the functions of the proposed converter. Based on the small-signal model, the mutual control system is demonstrated to have an excellent stability margin. The bidirectional dead-band logic is analyzed according to the output voltage change. The experimental results have verified the theoretical analysis.

References

[1] C. Liu, P. W. Sun, J. S. Lai, Y. C. Ji, M. Y. Wang, C. L. Chen, and G. W. Cai, "Cascade dual-boost/buck active-front-end converter for intelligent universal transformer," *IEEE Transactions on Industrial Electronics*, vol. 59, no. 12, pp. 4671–4680, Dec. 2012.

[2] L. Ferreira Costa, G. De Carne, G. Buticchi, and M. Liserre, "The smart transformer: a solid-state transformer tailored to provide ancillary services to the distribution grid," *IEEE Power Electronics Magazine*, vol. 4, no. 2, pp. 56–67, Jun. 2017.

[3] X. She, X. W. Yu, F. Wang, and A. Q. Huang, "Design and demonstration of a 3.6-kV–120-V/10-kVA solid-state transformer for smart grid application," *IEEE Transactions on Power Electronics*, vol. 29, no. 8, pp. 3982–3996, Aug. 2014.

[4] B. Zhao, Q. Song, J. G. Li, Q. H. Sun, and W. H. Liu, "Full-process operation, control, and experiments of modular high-frequency-link DC transformer based on dual active bridge for flexible MVDC distribution: a practical tutorial," *IEEE Transactions on Power Electronics*, vol. 32, no. 9, pp. 6751–6766, Sep. 2017.

[5] L. Wang, D. L. Zhang, Y. Wang, B. Wu, and H. S. Athab, "Power and voltage balance control of a novel three-phase solid-state transformer using multilevel cascaded H-Bridge inverters for microgrid applications," *IEEE Transactions on Power Electronics*, vol. 31, no. 4, pp. 3289–3301, Apr. 2016.

[6] Y. Wang, Q. Song, B. Zhao, J. G. Li, Q. H. Sun, and W. H. Liu, "Analysis and optimisation of modulation strategy based on dual-phase-shift for modular multilevel high-frequency-link DC transformer in medium-voltage DC distribution network," *IET Power Electronics*, vol. 11, no. 2, pp. 253–261, Feb. 2018.

[7] J. Q. Liu, J. X. Yang, J. P. Zhang, Z. Nan, and Q. L. Zheng, "Voltage balance control based on dual active bridge DC/DC converters in a power electronic traction transformer," *IEEE Transactions on Power Electronics*, vol. 33, no. 2, pp. 1696–1714, Feb. 2018.

[8] B. Zhao, Q. Song, and W. H. Liu, "A practical solution of high-frequency-link bidirectional solid-state transformer based on advanced components in hybrid microgrid," *IEEE Transactions on Industrial Electronics*, vol. 62, no. 7, pp. 4587–4597, Jul. 2015.

[9] M. N. Kheraluwala, R. W. Gascoigne, D. M. Divan, and E. D. Baumann, "Performance characterization of a high-power dual active bridge DC-to-DC converter," *IEEE Transactions on Industry Applications*, vol. 28, no. 6, pp. 1294–1301, Nov./Dec. 1992.

[10] A. Rodríguez, A. Vázquez, D. G. Lamar, M. M. Hernando, and J. Sebastián, "Different purpose design strategies and techniques to improve the performance of a dual active bridge with phase-shift control," *IEEE Transactions on Power Electronics*, vol. 30, no. 2, pp. 790–804, Feb. 2015.

[11] G. G. Oggier, R. Leidhold, G. O. Garcia, A. R. Oliva, J. C. Balda, and F. Barlow, "Extending the ZVS operating range of dual active bridge high-power DC-DC converters," in *2006 37th IEEE Power Electronics Specialists Conference*, Jeju, Korea (South), Jun. 2006, pp. 1–7.

[12] B. Zhao, Q. G. Yu, and W. X. Sun, "Extended-phase-shift control of isolated bidirectional DC–DC converter for power distribution in microgrid," *IEEE Transactions on Power Electronics*, vol. 27, no. 11, pp. 4667–4680, Nov. 2012.

[13] B. Zhao, Q. Song, and W. H. Liu, "Power characterization of isolated bidirectional dual-active-bridge DC–DC converter with dual-phase-shift control," *IEEE Transactions on Power Electronics*, vol. 27, no. 9, pp. 4172–4176, Sep. 2012.

[14] J. Huang, Y. Wang, Z. Q. Li, and W. J. Lei, "Multifrequency approximation and average modelling of an isolated bidirectional DC–DC converter for dc microgrids," *IET Power Electronics*, vol. 9, no. 6, pp. 1120–1131, May 2016.

[15] H. Bai, Z. L. Nie, and C. C. Mi, "Experimental comparison of traditional phase-shift, dual-phase-shift, and model-based control of isolated bidirectional DC–DC converters," *IEEE Transactions on Power Electronics*, vol. 25, no. 6, pp. 1444–1449, Jun. 2010.

[16] B. Zhao, Q. Song, W. H. Liu, and Y. D. Sun, "Overview of dual-active-bridge isolated bidirectional DC–DC converter for high-frequency-link power-conversion system," *IEEE Transactions on Power Electronics*, vol. 29, no. 8, pp. 4091–4106, Aug. 2014.

[17] B. Zhao, Q. Song, and W. H. Liu, "Efficiency characterization and optimization of isolated bidirectional DC–DC converter based on dual-phase-shift control for DC distribution application," *IEEE Transactions on Power Electronics*, vol. 28, no. 4, pp. 1711–1727, Apr. 2013.

[18] G. G. Oggier, G. O. García, and A. R. Oliva, "Switching control strategy to minimize dual active bridge converter losses," *IEEE Transactions on Power Electronics*, vol. 24, no. 7, pp. 1826–1838, Jul. 2009.

[19] A. K. Jain and R. Ayyanar, "PWM control of dual active bridge: Comprehensive analysis and experimental verification," *IEEE Transactions on Power Electronics*, vol. 26, no. 4, pp. 1215–1227, Apr. 2011.

[20] Y. D. Xiao, Z. Zhang, K. T. Manez, and M. A. E. Andersen, "A universal power flow model for dual active bridge-based converters with phase shift modulation," *IEEE Transactions on Power Electronics*, vol. 36, no. 6, pp. 6480–6500, Jun. 2021.

[21] Y. D. Xiao, Z. Zhang, M. A. E. Andersen, and K. Sun, "Impact on ZVS operation by splitting inductance to both sides of transformer for 1-MHz GaN based DAB converter," *IEEE Transactions on Power Electronics*, vol. 35, no. 11, pp. 11988–12002, Nov. 2020.

[22] Z. Zhang, J. S. Huang, and Y. D. Xiao, "GaN-based 1-MHz partial parallel dual active bridge converter with integrated magnetics," *IEEE Transactions on Industrial Electronics*, vol. 68, no. 8, pp. 6729–6738, Aug. 2021.

[23] N. Zhao, J. Q. Liu, Y. Ai, J. X. Yang, J. P. Zhang, and X. J. You, "Power-linked predictive control strategy for power electronic traction transformer," *IEEE Transactions on Power Electronics*, vol. 35, no. 6, pp. 6559–6571, Jun. 2020.

[24] J. Q. Liu, J. X. Yang, J. P. Zhang, Z. Nan, and Q. L. Zheng, "Voltage balance control based on dual active bridge DC/DC converters in a power electronic traction transformer," *IEEE Transactions on Power Electronics*, vol. 33, no. 2, pp. 1696–1714, Feb. 2018.

[25] Y. Wang, Z. D. Zheng, and Y. D. Li, "DAB-based PET in MVDC traction and shipboard applications with distribution and redundant control," *The Journal of Engineering*, vol. 2019, no. 16, pp. 3209–3213, Mar. 2019.

[26] P. Zumel, L. Ortega, A. Lázaro, C. Fernández, A. Barrado, A. Rodríguez, and M. M. Hernando, "Modular dual-active bridge converter architecture," *IEEE Transactions on Industry Applications*, vol. 52, no. 3, pp. 2444–2455, May/Jun. 2016.

[27] C. H. Zhao, D. Dujic, A. Mester, J. K. Steinke, M. Weiss, S. Lewdeni-Schmid, T. Chaudhuri, and P. Stefanutti, "Power electronic traction transformer—medium voltage prototype," *IEEE Transactions on Industrial Electronics*, vol. 61, no. 7, pp. 3257–3268, Jul. 2014.

[28] G. Ortiz, M. G. Leibl, J. E. Huber, and J. W. Kolar, "Design and experimental testing of a resonant DC–DC converter for solid-state transformers," *IEEE Transactions on Power Electronics*, vol. 32, no. 10, pp. 7534–7542, Oct. 2017.

[29] H. Li and Z. Y. Jiang, "On automatic resonant frequency tracking in *LLC* series resonant converter based on zero-current duration time of secondary diode," *IEEE Transactions on Power Electronics*, vol. 31, no. 7, pp. 4956–4962, Jul. 2016.

[30] M. Lee, C. S. Yeh, O. Yu, J. W. Kim, J. M. Choe, and J. S. Lai, "Modeling and control of three-level boost rectifier based medium-voltage solid-state transformer for DC fast charger application," *IEEE Transactions on Transportation Electrification*, vol. 5, no. 4, pp. 890–902, Dec. 2019.

[31] F. Liu, G. J. Zhou, X. B. Ruan, S. Y. Ji, Q. L. Zhao, and X. Y. Zhang, "An input-series-output-parallel converter system exhibiting natural input-voltage sharing and output-current sharing," *IEEE Transactions on Industrial Electronics*, vol. 68, no. 2, pp. 1166–1177, Feb. 2021.

[32] X. Y. Chen, G. Xu, S. M. Xie, H. Han, M. Su, Y. Sun, H. Wang, Y. L. Liu, and W. J. Xiong, "A natural bidirectional input-series–output-parallel LLC-DCX converter with automatic power sharing and power limitation capability for li-ion battery formation and grading system," *IEEE Journal of Emerging and Selected Topics in Power Electronics*, vol. 8, no. 4, pp. 3618–3632, Dec. 2020.

[33] R. L. Da Silva, V. L. F. Borges, C. E. Possamai, and I. Barbi, "Solid-state transformer for power distribution grid based on a hybrid switched-capacitor LLC-SRC converter: analysis, design, and experimentation," *IEEE Access*, vol. 8, pp. 141182–141207, Jul. 2020.

[34] K. Tan, R. Y. Yu, S. X. Guo, and A. Q. Huang, "Optimal design methodology of bidirectional LLC resonant DC/DC converter for solid state transformer application," in *IECON 2014–40th Annual Conference of the IEEE Industrial Electronics Society*, Dallas, TX, USA, Oct./Nov. 2014, pp. 1657–1664.
[35] T. Y. Jiang, J. M. Zhang, X. K. Wu, K. Sheng, and Y. S. Wang, "A bidirectional LLC resonant converter with automatic forward and backward mode transition," *IEEE Transactions on Power Electronics*, vol. 30, no. 2, pp. 757–770, Feb. 2015.
[36] W. L. Malan, D. M. Vilathgamuwa, and G. R. Walker, "Modeling and control of a resonant dual active bridge with a tuned CLLC network," *IEEE Transactions on Power Electronics*, vol. 31, no. 10, pp. 7297–7310, Oct. 2016.
[37] C. Liu, H. Y. Liu, G. W. Cai, S. M. Cui, H. J. Liu, and H. Yao, "Novel hybrid LLC resonant and DAB linear DC–DC converter: average model and experimental verification," *IEEE Transactions on Industrial Electronics*, vol. 64, no. 9, pp. 6970–6978, Sep. 2017.
[38] U. Kundu, K. Yenduri, and P. Sensarma, "Accurate ZVS analysis for magnetic design and efficiency improvement of full-bridge LLC resonant converter," *IEEE Transactions on Power Electronics*, vol. 32, no. 3, pp. 1703–1706, Mar. 2017.
[39] K. Zhang, Z. Y. Shan, and J. Jatskevich, "Large- and small-signal average-value modeling of dual-active-bridge DC–DC converter considering power losses," *IEEE Transactions on Power Electronics*, vol. 32, no. 3, pp. 1964–1974, Mar. 2017.
[40] E. X. Yang, F. C. Lee, and M. M. Jovanovic, "Small-signal modeling of series and parallel resonant converters," *APEC'92 Seventh Annual Applied Power Electronics Conference and Exposition*, Boston, MA, Feb. 1992, pp. 785–792.
[41] H. S. Qin and J. W. Kimball, "Generalized average modeling of dual active bridge DC–DC converter," *IEEE Transactions on Power Electronics*, vol. 27, 27, no. 4, pp. 2078–2084, Apr. 2012.
[42] S. Zong, H. Z. Luo, W. H. Li, X. N. He, and C. L. Xia, "Theoretical evaluation of stability improvement brought by resonant current loop for paralleled LLC converters," *IEEE Transactions on Industrial Electronics*, vol. 62, no. 7, pp. 4170–4180, Jul. 2015.
[43] J. Tian, J. Petzoldt, T. Reimann, M. Scherf, and G. Berger, "Envelope model of frequency-duty-controlled LLC converters," in *2007 IEEE Power Electronics Specialists Conference*, Orlando, FL, USA, Jun. 2007, pp. 876–881.
[44] J. H. Jung, H. S. Kim, M. H. Ryu, and J. W. Baek, "Design methodology of bidirectional CLLC resonant converter for high-frequency isolation of DC distribution systems," *IEEE Transactions on Power Electronics*, vol. 28, no. 4, pp. 1741–1755, Apr. 2013.

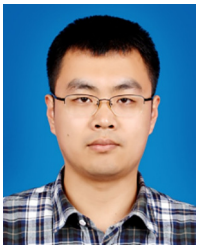

Haiyang Liu received a B.S. degree in Electrical Engineering from Huazhong University of Science and Technology, Wuhan, China in 2011 and a M.S. degree in Electrical Engineering from Northeast Electric Power University, Jilin, China in 2014. From 2018 to 2020, he was with Emergy Technology (ET), Aalborg University (AAU), Denmark, as a Visiting Ph.D. Student, supported by the Chinese Scholarship Council. He is currently working toward a Ph.D. degree in Electrical Engineering at Harbin Institute of Technology (HIT), Harbin, China. His research interests are related to power electronic energy conversion based on the future smart grid with abundant renewable energy.

Shumei Cui received a Ph.D. degree in Electrical Engineering from Harbin Institute of Technology (HIT), Harbin, China, in 1998. She has been a Professor with the Department of Electrical Engineering, HIT, where she is also currently the Vice Dean of the Institute of Electromagnetic and Electronic Technology and the Dean of the Electric Vehicle Research Center. Her research interests include design and control of micro and special electric machines, electric drive systems of electric vehicles, control and simulation of hybrid electric vehicles, and intelligent test and fault diagnostics of electric machines. Dr. Cui serves as the Vice Director of the Micro and Special Electric Machine Committee of the Chinese Institute of Electronics, and is a member the Electric Vehicle Committee and the National Automotive Standardization Technical Committee.

Hanwen Zhang received B.Sc. and M.Sc. degrees in Electrical Engineering from Northeast Electric Power University, Jilin, Jilin, China, in 2017 and 2020. In 2018, he was a Visiting Student at Cardiff University, Cardiff, UK. Since 2021, he has been working toward a Ph.D. degree with Aalborg University, Aalborg, Denmark. His research interests include power electronics and power electronics intensive applications in MVDC/LVDC grid.

Yiwen Hu received a B.S. degree from Northeast Electric Power University, Jilin, China, in 2020. She is currently working toward an M.S. degree in Electrical Engineering at Northeast Electric Power University, Jilin, China. Her current research interests include high frequency isolated DC-AC inverters, and the microgrid.

Yuhongyang Xue is currently studying for a bachelor's degree in Electrical Engineering and Automation at the School of Electrical Engineering and Automation, Northeast Electric Power University, Jilin, China.

Chuang Liu received an M.S. degree in Electrical Engineering in 2009 from Northeast Electric Power University, China, and a Ph.D. degree from Harbin Institute of Technology, Harbin, China, in 2013. From 2010 to 2012, he was with the Future Energy Electronics Center (FEEC), Virginia Tech, Blacksburg, as a Visiting Ph.D. Student, supported by the Chinese Scholarship Council. In 2013, he joined Northeast Electric Power University as an Associate Professor with the School of Electrical Engineering, Jilin, China. Since 2016, he has been a professor. His research interests are related to power electronics based AC and DC transformers for the future hybrid AC/DC power grid, modular AC-DC inverters for battery energy storage systems, power electronics based power system stability analysis and control.